Technical Note

Quantitative 3D Trajectory Measurement for Percutaneous Endoscopic Lumbar Discectomy

Xin Huang, MD, Bin Zhu, MD, and Xiaoguang Liu, MD

From: Pain Medicine Center and Department of Orthopedics, Peking University Third Hospital, Beijing, China

Address Correspondence:
Xiaoguang Liu, MD
Pain Medicine Center and Department of Orthopedics
Peking University Third Hospital
No. 49, North Garden Road
Haidian District, Beijing 100191, P. R. China
E-mail: zhubin_ortho@163.com

Disclaimer: Dr. Huang and Dr. Zhu contributed equally to this work and share the first authorship. This work was supported by The National Key Research and Development Program of China (2017YFC0108100).

Manuscript received: 09-15-2017
Revised manuscript received: 12-02-2017
Accepted for publication: 01-10-2018

Free full manuscript: www.painphysicianjournal.com

Background: Percutaneous endoscopic lumbar discectomy (PELD) has become an increasingly popular minimally invasive spinal surgery. Due to the technical evolution of PELD, the focus of decompression has shifted from the central nucleus to the subannular-protruded disc herniation, which allows direct neural decompression. Surgical entry into the spinal canal leads to the greater possibility of bony structure obstruction, thus the location and direction of the working channel are crucial. The existing preoperative measuring methods mainly rely on 2-dimensional (2D) x-ray images or MRI cross-sections. Because the bony structure and the trajectory are 3-dimensional (3D), the relationship between the anatomical lumbar structure and the working channel cannot be precisely evaluated.

Objectives: To investigate a 3D method and quantitatively evaluate the trajectory for percutaneous endoscopic lumbar discectomy (PELD).

Study Design: Technical note.

Setting: Pain medicine center of a university hospital.

Methods: Twenty patients suffering from L4/5 disc herniation were enrolled in this study. After reconstructing the preoperative CT images, the virtual trajectory was placed into the intervertebral foramen through gradient-changing angulations in relation to the coronal and transverse planes. The overlapping portion of the virtual trajectory and the lumbar vertebrae was evaluated. In addition, the probability of atypical structure involvement was calculated.

Results: As cephalad angulation (CA) increased, the intersection volume of the L4 inferior articular process increased, while the total intersection volume, the intersection volume of the L5 superior articular process, the intersection volume of the facet joint, and the volume proportion of L5 superior articular process intersection in the facet joint all decreased. As coronal plane angulation (CPA) increased, the total intersection volume, the intersection volume of the L4 inferior articular process, and the intersection volume of the facet joint all increased, while the volume proportion of the L5 superior articular process intersection in the facet joint decreased. When CA increased to 15°-20°, there was a high probability of atypical structure involvement, whereas such a probability in the groups of CA 0° (CPA 15°, 20°, and 25°), CA 5° and CA 10° was low.

Limitations: Only patients with L4/5 herniation were evaluated in this study.

Conclusions: In terms of the regularity, the ideal angulation for L4/L5 PELD is CPA 5°-10° and CA 5°-10°, which can lead to a relatively low level of total damage to the bony structure, minimal damage to the facet joint, and negligible involvement of atypical structures.

Key words: Lumbar disc herniation, percutaneous endoscopic lumbar discectomy (PELD), transforaminal, trajectory, 3D method, quantitative measurement, angulation, bony structure obstruction

Pain Physician 2018; 21:E355-E365

Percutaneous endoscopic lumbar discectomy (PELD) has become increasingly popular in minimally invasive spinal surgery. As described by Kambin et al (1), the PELD procedure was first devised for treating contained soft disc herniation. Subsequently, Yeung developed the Yeung Endoscopic Spine System (YESS) (2), which was characterized by puncturing into the target disc to achieve indirect neural decompression. However, the methods and techniques of PELD have changed remarkably. In 2006, Hoogland proposed a transforaminal endoscopic spine system (TESSYS) (3,4), which was characterized by a step-by-step foraminoplasty using special reamers to enlarge the intervertebral foramen, thus making it possible to operate inside the spinal canal. Since then, the focus of decompression has shifted from central nucleus to subannular-protruded disc herniation (5), which enables direct neural decompression. Along with the technical evolution, the surgical indications of PELD have been expanded to include uncontained disc herniation (6), highly migrated fragments (7), sequestrated fragments (8), and even lumbar spinal stenosis (9,10).

Surgical entry into the spinal canal leads to the greater possibility of bony structure obstruction, thus the location and direction of the working channel are crucial. An optimal trajectory ensures the successful entry of the cannulated obturator, endoscope, and other relevant instruments into the intervertebral foramen (11), whereas an inaccurate orientation can lead to a higher fluoroscopy frequency, longer operation time, and an incomplete view, thus increasing the risk of complications (5,12).

Currently, the selection of the entry point is length-dependent (2,4) (for example, 12-14 cm from the midline at the L4/L5 level when using the TESSYS technique). Since the body sizes of individual patients are different, the puncture and localization procedures mainly rely on the experience of the operators, making it one of the most difficult steps for beginners in performing PELD (13). The existing preoperative measuring methods mainly rely on 2-dimensional (2D) X-ray images or MRI cross-sections (14). Because the bony structure and the trajectory are 3-dimensional (3D), the relationship between the anatomical lumbar structure and the working channel cannot be evaluated precisely.

In our study, a 3D method was developed to quantitatively evaluate the trajectory for PELD. After reconstructing the preoperative CT images of the patients, the virtual trajectory was placed into the intervertebral foramen through gradient-changing angulations in relation to the coronal and transverse planes. The specific anatomical structure involved by the virtual trajectory was evaluated, and the volume of intersection was quantitatively calculated. The results clarify the regularity between the puncture trajectory and the lumbar spine, thus helping to select an ideal trajectory for PELD.

Methods

Patient Characteristics

A total of 76 patients suffering from lumbar disc herniation were admitted to the hospital between March 2015 and June 2015. The inclusion criterion was the presence of L4/5 lumbar disc herniation, which was diagnosed using MRI and was manifested as radicular pain or progressive neurologic deficit that was unresponsive to conservative therapies. The exclusion criteria included concomitant herniation at other lumbar levels, spinal stenosis, calcified disc, segmental instability, and cauda equina syndrome. According to the criteria, 20 patients (16 males and 4 females) were ultimately enrolled in this study. The age of the patients ranged from 14 to 72 years old (with a mean age of 39.9 years).

Reconstruction of a 3D Model

The study protocol was approved by the local institutional review board. All patients signed an informed consent document. Before the PELD surgery, lumbar computed tomography (SOMATOM Definition Flash CT; SIEMENS Healthineers, Erlangen, Germany) with 1mm slice thickness was performed on all patients. The digital imaging and communications in medicine (DICOM) data were acquired and reconstructed using the MIMICS 17.0 software (Materialise, Leuven, Belgium). During the reconstruction, thin-layer CT axial images were first imported into the software. The bone segmentation was completed using the "CT bone segmentation toolkit." The masks of L4 and L5 were then specified and reconstructed by 3D rendering using the "Calculate 3D" function with high quality.

Virtual Trajectory Placement and Measurement

A cylindrical region (radius = 4mm, length = 150mm, based on the size of commonly used cannulated obturators) was established as the virtual trajectory and was converted into the Standard Template Library (STL) data format. The transverse plane and the coronal plane were marked by the MIMICS 17.0 software automatically according to the patients' original CT data.

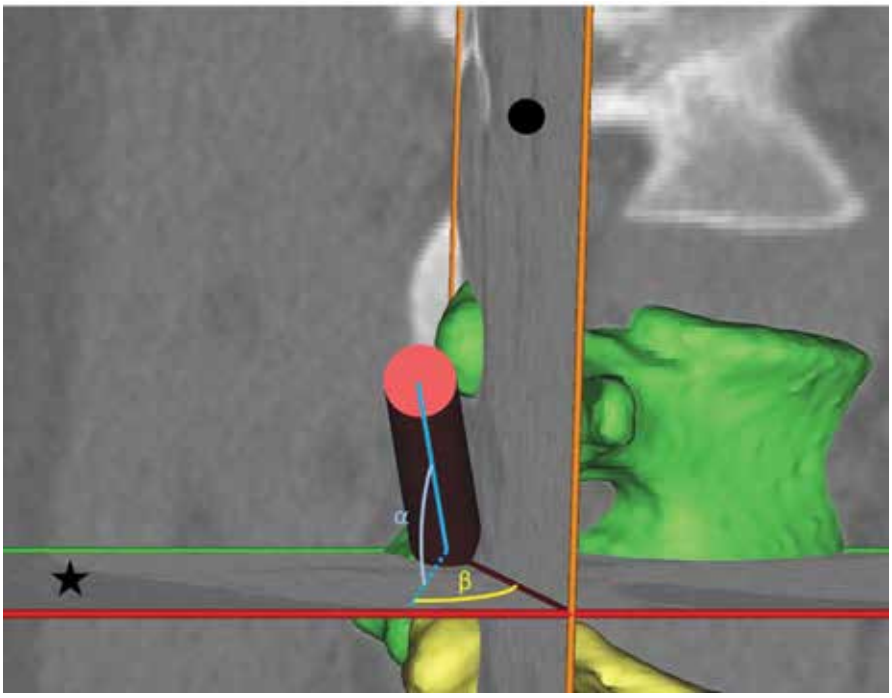

Fig. 1. *Illustration of the relationship between the virtual trajectory and the anatomic plane. ★: transverse plane; ●: coronal plane; α: cephalad angulation (CA), defined as the angle between the virtual trajectory and the transverse plane; β: coronal plane angulation (CPA), defined as the angle between the virtual trajectory and the coronal plane.*

The cephalad angulation (CA) of the virtual trajectory was defined as the angle between the virtual trajectory and the transverse plane, and the coronal plane angulation (CPA) was defined as the angle between the virtual trajectory and the coronal plane (Fig. 1). The target point was defined as the midpoint between the posterior edges of the L4 and L5 vertebral bodies in both the transverse plane and the sagittal plane. The initial conditions of the trajectory were configured as follows (Fig. 2): the CPA was 0°, the CA was 0°, and the target point was located on the ventral boundary of the terminal cylinder at the central level.

The overlapping portion between the virtual trajectory and the lumbar vertebrae was analyzed (Fig. 3). After cutting along specific planes, the overlapping portion was divided into several parts according to the microanatomical structure of the lumbar vertebrae. The intersection volumes of the L4 vertebrae, the L5 vertebrae, the L5 superior articular process, and the L4 inferior articular process were determined and recorded. The total intersection volume, the intersection volume of the facet joint , the volume proportion of the L5 superior articular process intersection in the facet joint, the ratio between the intersection volume of the facet joint and the total intersection volume were calculated. In addition, the probability of involvement by atypical structures (the bony structures that were not supposed to hinder the standard trajectory, including pedicle, transverse process, accessory process, and pars interarticularis) were evaluated.

According to the results of preliminary experiments, the cylindrical region was rotated to a series of predefined angulations in sequence (CPA: 0°, 5°, 10°, 15°, 20°, and 25°; CA: 0°, 5°, 10°, 15°, and 20°). The above evaluation procedures were repeated for every angulation group. All the measurements were carried out twice and the data were averaged.

Statistical Analysis

Experimental data were expressed as mean ± standard error (SE). Statistical analysis was performed using Pearson correlation with 2 dependent variables. All statistical computations were performed using SPSS software (version 18.0, SPSS Inc., Chicago, IL, USA). A *P* value of < 0.05 in 2-tailed tests was considered statistically significant.

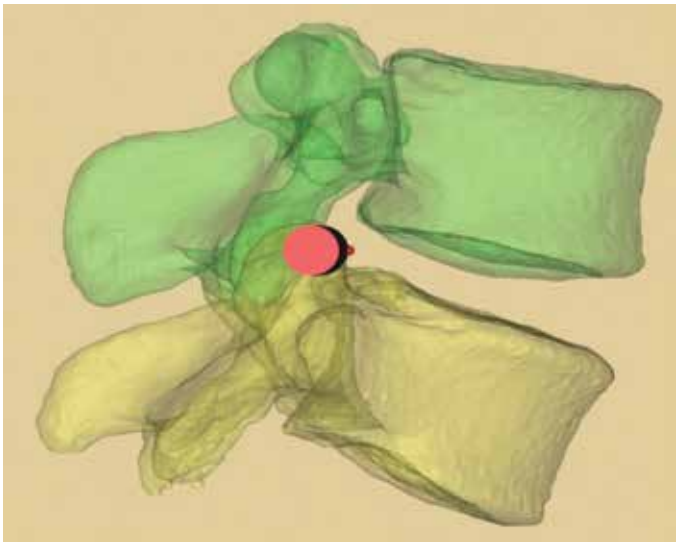

Fig. 2. *The initial condition of the trajectory. Red dot: the target point.*

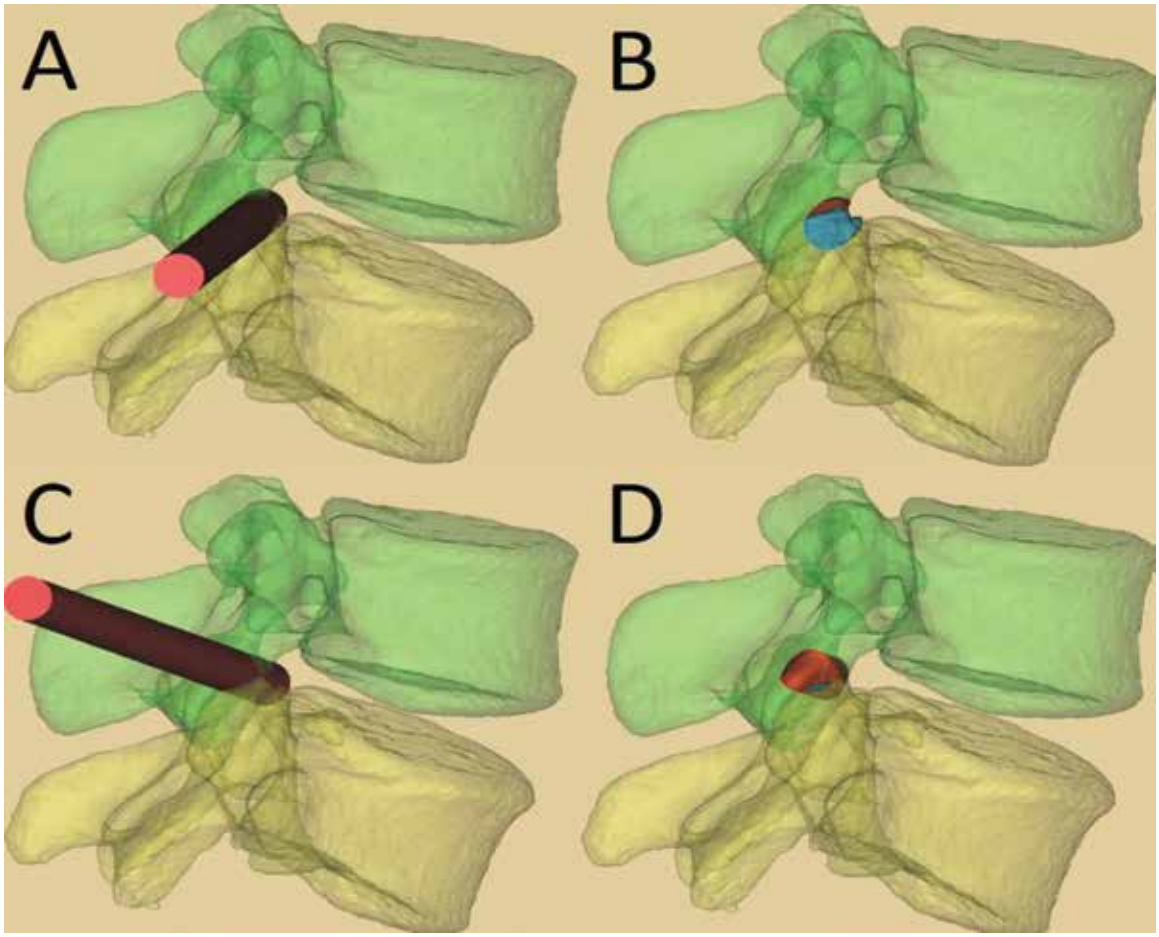

Fig. 3. *Illustration of the virtual trajectory (A and C) and the overlapping portion between the virtual trajectory and the lumbar vertebrae (B and D). A and B: CA 5° and CPA 5°; C and D: CA 15° and CPA 15°; Green area: L4; yellow area: L5; red area: overlapping portion between the virtual trajectory and L4; blue area: overlapping portion between the virtual trajectory and L5.*

Results

Measurement of Intersection Volumes

The variation in the total intersection volume is shown in Fig. 4. Generally, when CA was a constant, the total intersection volume increased significantly with an increasing value of CPA (r = 0.511, $P < 0.001$). When CPA was a constant, the total intersection volume decreased as CA increased from 0-15° (r = -0.375, $P < 0.001$).

The variation in the intersection volume of the L4 inferior articular process is shown in Fig. 5, and the variation in the intersection volume of the L5 superior articular process is shown in Fig. 6. The involvement of the L4 inferior articular process was mainly affected by CPA. In each CA group, the intersection volume of the L4 inferior articular process increased significantly with an increased value of CPA (r = 0.699, $P < 0.001$). When CPA was a constant, the intersection volume of the L4 inferior articular process slightly increased with an increased value of CA (r = 0.109, $P = 0.007$). The involvement of the L5 superior articular process was mainly affected by CA. When CPA was a constant, the intersection volume of the L5 superior articular process significantly decreased with an increased value of CA (r = -0.652, $P < 0.001$). In each CA group, the intersection volume of the L5 superior articular process initially increased and then decreased (r = -0.103, $P = 0.012$). The variation in the intersection volume of the facet joint is shown in Fig.7. The intersection volume of the facet joint increased significantly with a decreased value of CA (r = -0.503, $P < 0.001$) or an increased value of CPA (r = 0.501, $P < 0.001$).

Proportion of the Intersection Volume

The variation in the volume proportion of the L5 superior articular process intersecting in the facet joint is shown in Fig. 8. The volume proportion of the L5 superior articular process intersection in the facet joint decreased significantly with an increased value of CA (r = -0.415, $P < 0.001$) or CPA (r = -0.559, $P < 0.001$). Figure 9 shows the ratio between the intersection volume of the facet joint and the total intersection volume. When CA was low, the ratio was nearly 100%. As the value of CA increased, some atypical structures were involved. In the CA 15° and CA 20° groups, the ratio increased with an increased value of CPA (r = 0.238, $P < 0.001$).

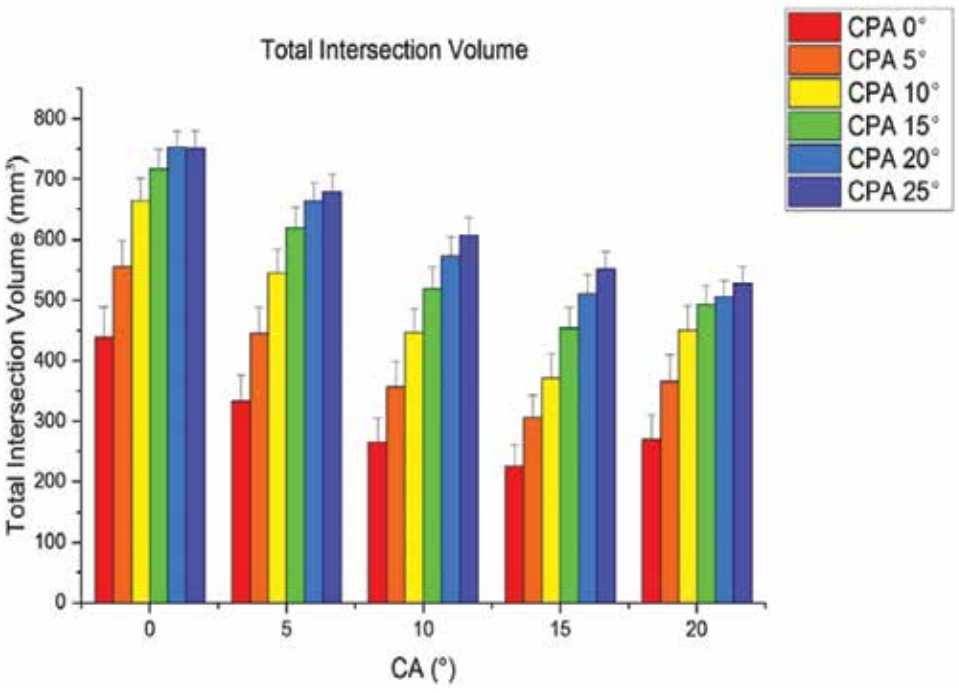

Fig. 4. *A bar graph showing the variation in the total intersection volume. CA, cephalad angulation; CPA, coronal plane angulation. CPA: r = 0.511, P < 0.001; CA: r = -0.375, P < 0.001.*

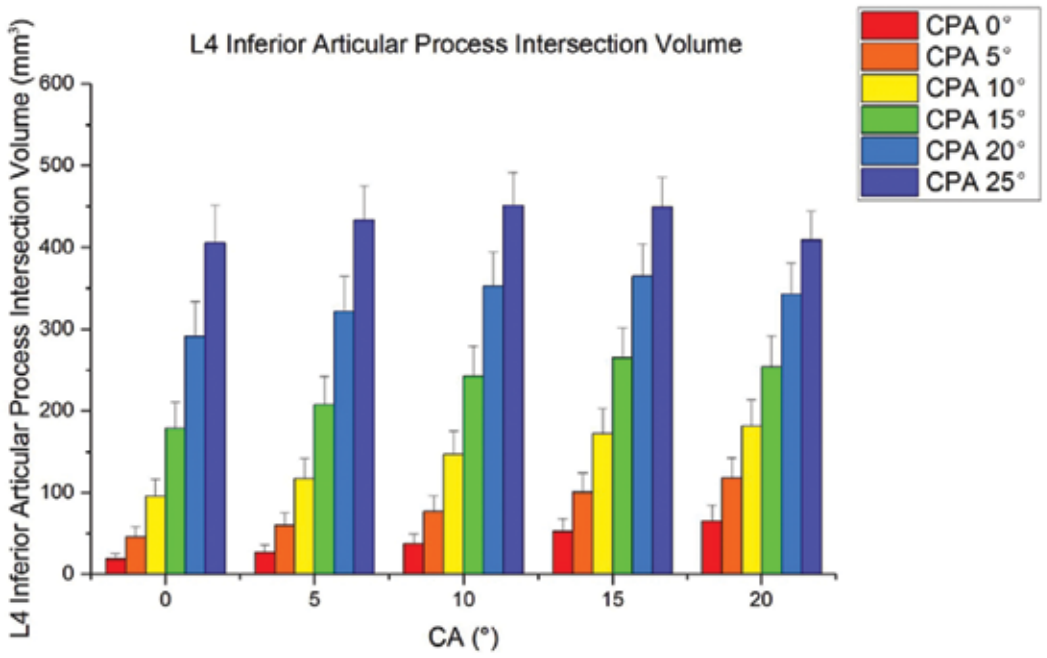

Fig. 5. *A bar graph showing the variation in the intersection volume of the L4 inferior articular process. CPA: r = 0.699, P < 0.001; CA: r = 0.109, P = 0.007.*

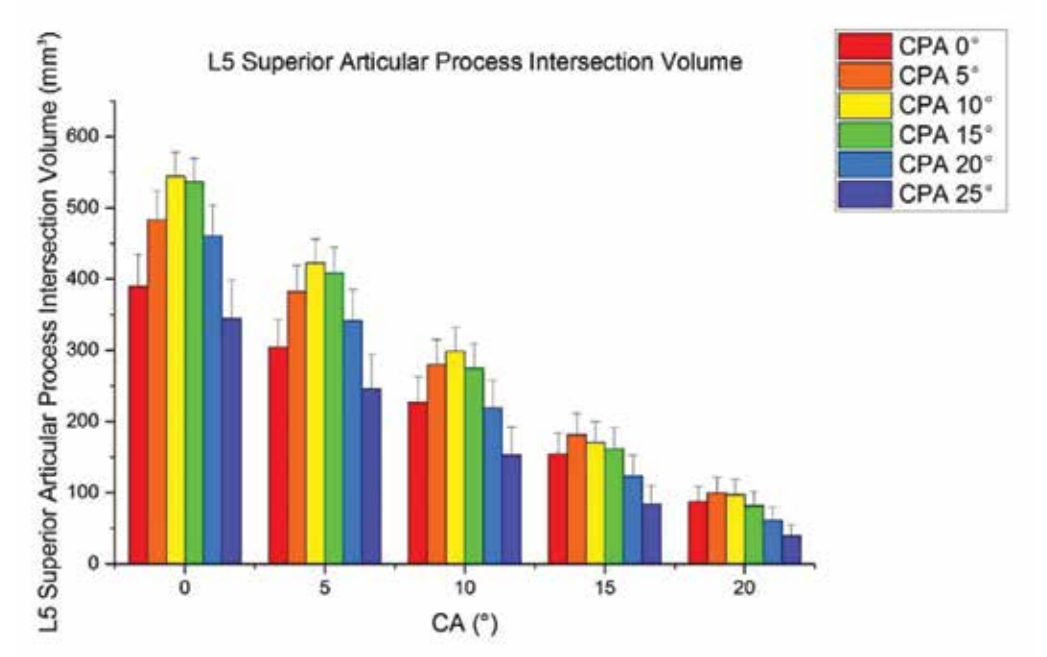

Fig. 6. *A bar graph showing the variation in the intersection volume of the L5 superior articular process. CPA: r = -0.103, P = 0.012; CA: r = -0.652, P < 0.001.*

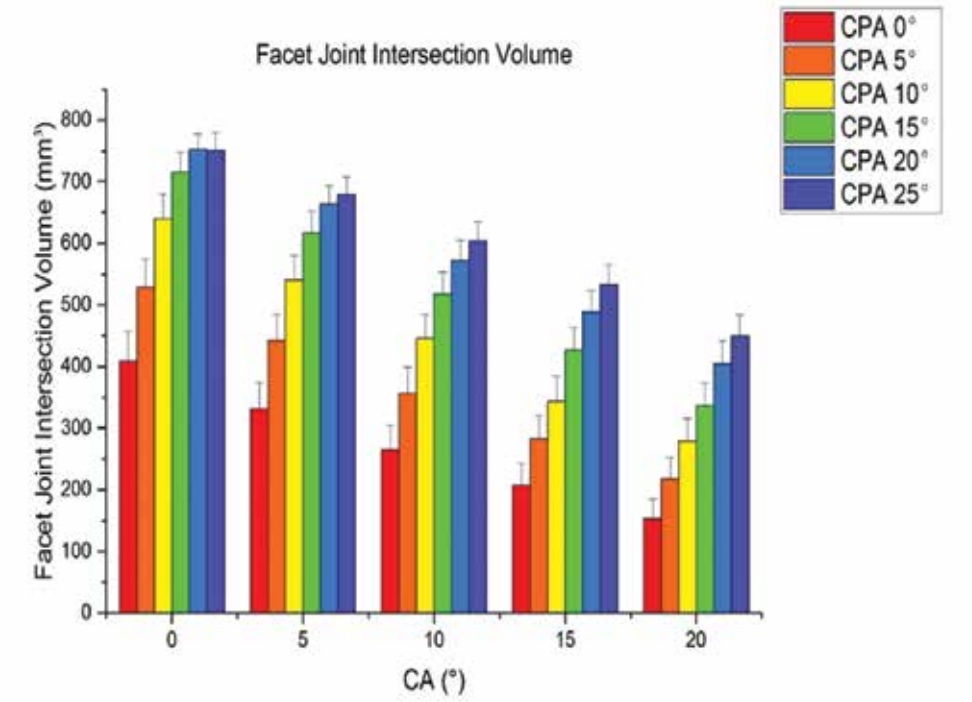

Fig. 7. *A bar graph showing the variation in the intersection volume of the facet joint. CPA: r = 0.501, P < 0.001; CA: r = -0.503, P < 0.001.*

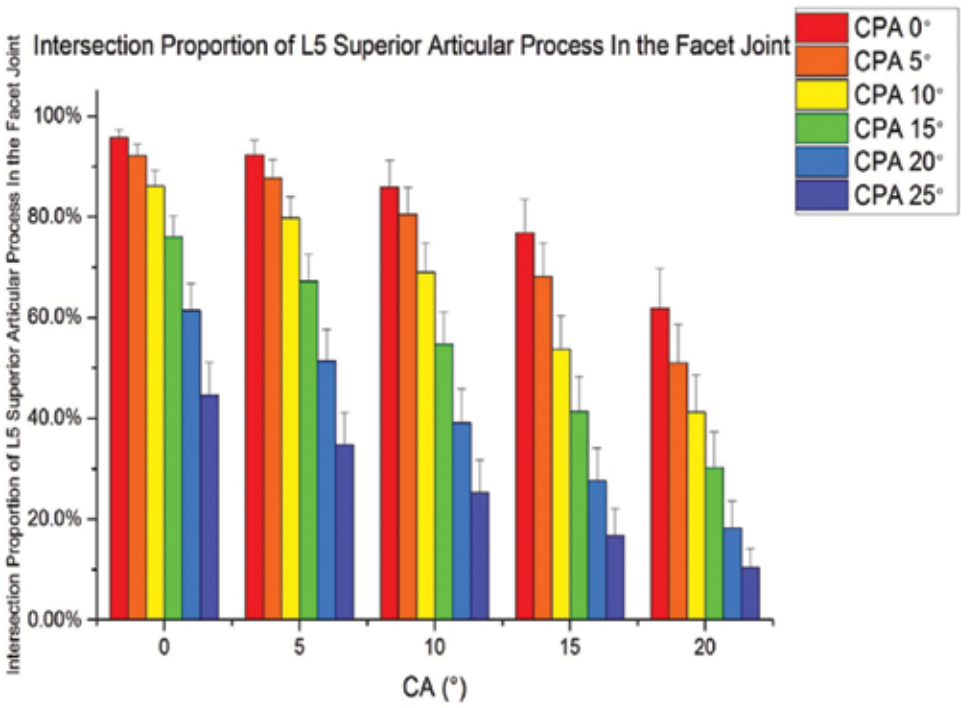

Fig. 8. A bar graph showing the variation in the intersecting proportion of the L5 superior articular process in the facet joint. CPA: r = -0.559, P < 0.001; CA: r = -0.415, P < 0.001.

Involvement of Atypical Structures

The probability of atypical structure involvement is shown in Table 1. When CA was low, there was a low probability that the virtual trajectory might involve the L5 pedicle or transverse process. Elevation of the CA value reduced the probability of L5 atypical structures involvement but increased the involvement by L4 atypical structures. In the CA15° and CA20° groups, when CPA was low, the virtual trajectory might involve the L4 pedicle and transverse processes. As the value of CPA increased, the probability of involvement by the L4 pedicle and the transverse processes decreased, whereas the probability of involvement by the L4 accessory process and the L4 pars interarticularis increased.

Discussion

Current Knowledge about Trajectory Selection

The establishment of an optimal working channel is one of the most critical steps in PELD. In the techniques of YESS (2) and TESSYS (4), the trajectory selection mainly relies on one anteroposterior fluoroscopy and one lateral fluoroscopy. Choi proposed a preoperative method to use the markers on the patients' body surface to evaluate the MRI cross-sectional images and to subsequently select the optimal entry point based on the following simple standards: 1) the safety of the puncture track, and 2) the convenience of reaching the target (11). However, the cross-section evaluation is still based on 2D images, whereas the bony structure and trajectory are 3D. Chen later proposed a preoperative 3D planning method to find an ideal path for transforaminal endoscopic surgery (15). However, because the resulting path was set to be a line segment rather than a cylinder, the involvement of the bony structure along the trajectory could not be evaluated precisely.

Standards for an Ideal Trajectory

After conducting measurements in gradient-changing angulations, an optimal trajectory for PELD operations was accessed. The standards for an ideal working channel in L4/5 PELD may include: 1) minimal damage to the bony structures (a small volume of total intersection); 2) maintenance of spinal stability with minimal damage to the facet joint (mainly involving

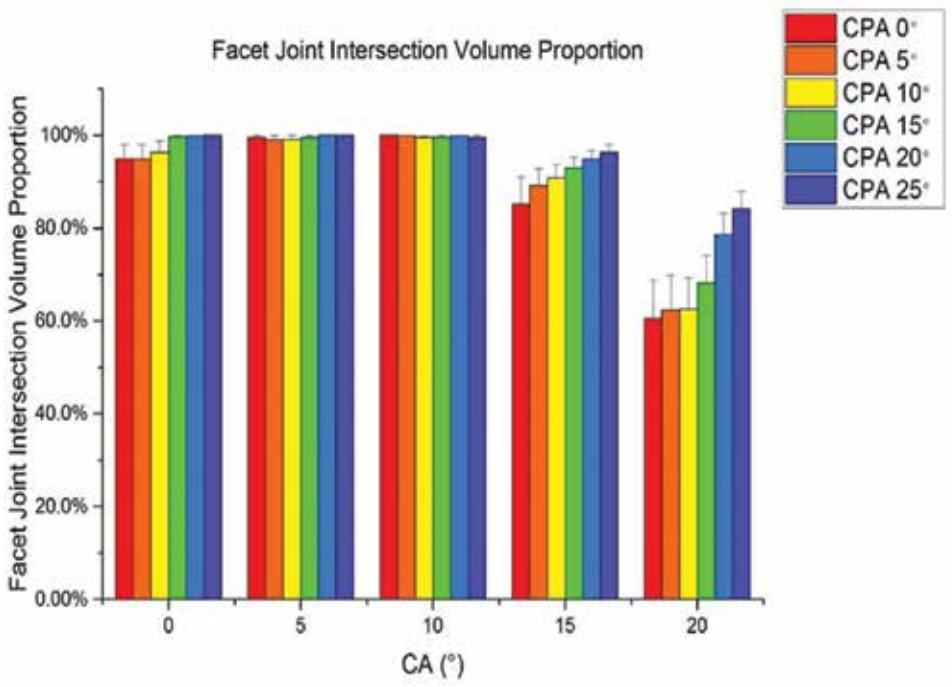

Fig. 9. *A bar graph showing the variation in the ratio between the intersection volume of the facet joint and total intersection volume. The ratio was close to 100% when the value of CA was low. In the groups of CA 15° and CA 20°, the ratio increased with an increased value of CPA ($r = 0.238$, $P < 0.001$).*

Table 1. *The probability of involvement by atypical structures at different angulations.*

	CA				
	0°	5°	10°	15°	20°
CPA 0°	L5 P 10% L5 TP 15%	L5 TP 10%	L4 P 5% L4 TP 10%	L4 P 10% L4 TP 30% L4 AP 10% L4 PI 15%	L4 P 25% L4 TP 70% L4 AP 15% L4 PI 45%
CPA 5°	L5 P 10% L5 TP 20%	L5 TP 10%	L5 TP 5% L4 TP 5% L4 AP 5%	L4 P 10% L4 TP 50% L4 AP 20% L4 PI 20%	L4 P 15% L4 TP 75% L4 AP 35% L4 PI 55%
CPA 10°	L5 TP 15%	L5 TP 10%	L4 TP 5% L4 AP 5%	L4 TP 50% L4 AP 30% L4 PI 45%	L4 TP 70% L4 AP 45% L4 PI 70%
CPA 15°	L5 TP 10%	L5 TP 10%	L4 TP 5% L4 AP 10%	L4 TP 30% L4 AP 40% L4 PI 45%	L4 TP 45% L4 AP 60% L4 PI 80%
CPA 20°	L5 TP 5%	None	L4 AP 20%	L4 TP 5% L4 AP 35% L4 PI 65%	L4 TP 30% L4 AP 60% L4 PI 85%
CPA 25°	None	None	L4 AP 10%	L4 AP 20% L4 PI 70%	L4 AP 45% L4 PI 80%

P, pedicle; TP, transverse Process; AP, accessory process; PI, pars interarticularis.

the L5 superior articular processes rather than the L4 inferior articular processes); 3) minimal obstruction by atypical structures, such as the L5 transverse process, the L4 pedicle and transverse processes, the L4 accessory processes, and the L4 pars interarticularis; and 4) the safety of the puncture track (avoiding critical spinal nerves and blood vessels).

Relationship between Trajectory Angulation and Bony Structures

The concept of minimally invasive surgery not only refers to a small skin incision, but also includes a limited destruction of the internal tissues. One of the advantages of PELD is the minimal damage to bony structures (16). Such damages can be evaluated by the intersection volumes in this study, because the cylindrical region (radius = 4mm, length = 150mm) indicated the space required by the commonly used cannulated obturators (outside diameter = 8.0mm). The results indicated that a decreased value of CPA and an increased value of CA could reduce the total damage (Fig. 3). However, a small volume of total intersection was not the sole standard, and other factors such as the facet joint and the exiting spinal nerves should also be considered.

As the decompression focus has been shifted from central nucleus to intra-canal herniation, foraminoplasty is sometimes necessary for surgical instruments to enter the spinal canal (5). The foraminoplasty procedure mainly focuses on the facet joint, especially on the ventral part of the superior articular process (6). Precise foraminoplasty can maintain spinal stability and provide adequate operational space at the same time. To our knowledge, no previous studies have reported the relationship between the trajectory angulation and the involvement of the facet joint. In our experiment, an excessive intersection volume of the L4 inferior articular process and a small volume proportion of the L5 superior articular process intersection in the facet joint were indications of the damage to the facet joint. The elevation in the values of CPA and CA has resulted in the increased intersection volume of the L4 inferior articular process (Fig. 5) and the decreased volume proportion of the L5 superior articular process intersection in the facet joint (Fig. 8). As a result, the reduction in the values of CPA and CA could minimize the damage to the facet joint. However, a minimal CA could lead to a maximal damage to the L5 superior articular process (Fig. 6) and the total bony structure (Fig. 4). A slight elevation in the CA value (for example, from CA0° to CA10°) may greatly reduce the damage to the L5 superior articular process (Fig. 6), and maintain a relatively intact facet joint at the same time.

Apart from the facet joint, other bony microstructures of the vertebrae (such as the L5 transverse pro-

cesses, the L4 pedicles and transverse processes, the L4 accessory processes, and the L4 pars interarticularis) may block the working channel. The results showed that a large CA value could result in a high probability of atypical structure involvement (Table 1). The reduction in CA resulted in less abnormal structures involvement. In the group of CA0° (CPA0°, 5°, and 10°), the ratio between the intersection volume of the facet joint and the total intersection volume was not 100% (Fig. 8) due to the involvement of the L5 pedicle and transverse processes. In the groups of CA0° (CPA15°, 20°, and 25°), CA5°, and CA10°, although the probability of atypical structure involvement was not completely eliminated (Table 1), the proportion of such involvement was negligible (Fig. 9). Thus these parameters were considered as candidates for the optimal angulation.

Moderate bony structure damage is acceptable in PELD, whereas even minor damage to the spinal nerve should be avoided. Avoidance of the exiting nerve is an important factor during trajectory planning. The spinal nerves exit the spinal canal through the superior part of the intervertebral foramen (1), along with the associative arteries. The incidence of exiting root damage has been reported to be 1.0% to 6.7% (17). Such injury usually results in postoperative dysesthesia and motor weakness. Although it is not life-threatening, the damage hinders a quick recovery and reduces patient satisfaction. Choi et al (17) confirmed that the distance from the exiting root to the facet at the lower disc level, as measured by a preoperative MRI scan, was relevant to the exiting root injury. Although the CT reconstruction images in our study did not show the exiting root directly, it was confirmed that when the value of CA was high, an increased value of CPA reduced the incidence of L4 pedicle involvement (Table 1) and increased the proportion of the facet joint intersection volume (Fig. 8). Both these parameters were representative of less compression to the superior part of the intervertebral foramen. These results were consistent with those of the previous studies, which have demonstrated that the working cannula should be placed as close to the facet joint as possible in order to avoid an exiting root injury (18). In addition to the surgical technique, sufficient intraoperative communication with the patient under local anesthesia is also important.

In terms of the regularity, the ideal angulation for L4/L5 PELD is CPA 5°-10° and CA 5°-10°, which can lead to a relatively low level of total damage to the bony structure, minimal damage to the facet joint, and negligible involvement of atypical structures. The regularity between the dynamic trajectory and the lumbar vertebral structure has been summarized in terms of multiple patients and can improve the understanding about working channel establishment. As for one specific patient, the 3D preoperative planning method presented in our study is helpful for specialized trajectory designing. The preliminary results presented in this article may be useful for the future design and application of surgical navigation tools, surgical robots, and artificial intelligence applications during PELD surgery.

Limitations

This study has certain limitations. First, only patients with L4/5 herniation were evaluated, whereas herniation at other levels (such as L5/S1) was not included. Moreover, the theoretical regularity was summarized in terms of the preoperative data, while further clinical experiments are needed to evaluate its clinical efficacy. In addition, the 3D reconstruction method presented in this study is mainly based on the CT data and could not be used to evaluate the spinal nerve directly. In the future, a MRI/CT fusion technique is expected to solve this problem.

Conclusion

Entry into the spinal canal during PELD enables direct neural decompression while introducing a greater risk for bony structure obstruction at the same time. In this study, a preoperative 3D method was proposed for planning the working channel. The relationship between the bony structure involvement and the trajectory was evaluated quantitatively. In terms of regularity, the ideal angulation for L4/L5 PELD is CPA 5°-10° and CA 5°-10°, which can lead to a relatively low level of total damage to the bony structure, minimal damage to the facet joint, and negligible involvement of atypical structures.

Acknowledgments

This work was supported by The National Key Research and Development Program of China (2017YFC0108100).

References

1. Kambin P, Brager MD. Percutaneous posterolateral discectomy. Anatomy and mechanism. *Clin Orthop Relat Res* 1987; 223:145-154.
2. Yeung AT, Tsou PM. Posterolateral endoscopic excision for lumbar disc herniation: Surgical technique, outcome, and complications in 307 consecutive cases. *Spine (Phila Pa 1976)* 2002; 27:722-731.
3. Hoogland T, Schubert M, Miklitz B, Ramirez A. Transforaminal posterolateral endoscopic discectomy with or without the combination of a low-dose chymopapain: A prospective randomized study in 280 consecutive cases. *Spine (Phila Pa 1976)* 2006; 31:E890-897.
4. Hoogland T, van den Brekel-Dijkstra K, Schubert M, Miklitz B. Endoscopic transforaminal discectomy for recurrent lumbar disc herniation: A prospective, cohort evaluation of 262 consecutive cases. *Spine (Phila Pa 1976)* 2008; 33:973-978.
5. Ahn Y. Transforaminal percutaneous endoscopic lumbar discectomy: Technical tips to prevent complications. *Expert Rev Med Devices* 2012; 9:361-366.
6. Li ZZ, Hou SX, Shang WL, Song KR, Zhao HL. Modified percutaneous lumbar foraminoplasty and percutaneous endoscopic lumbar discectomy: instrument design, technique notes, and 5 years follow-up. *Pain Physician* 2017; 20:E85-85E98.
7. Ahn Y, Jang IT, Kim WK. Transforaminal percutaneous endoscopic lumbar discectomy for very high-grade migrated disc herniation. *Clin Neurol Neurosurg* 2016; 147:11-17.
8. Schubert M, Hoogland T. Endoscopic transforaminal nucleotomy with foraminoplasty for lumbar disk herniation. *Oper Orthop Traumatol* 2005; 17:641-661.
9. Wen B, Zhang X, Zhang L, Huang P, Zheng G. Percutaneous endoscopic transforaminal lumbar spinal canal decompression for lumbar spinal stenosis. *Medicine (Baltimore)* 2016; 95:e5186.
10. Li ZZ, Hou SX, Shang WL, Cao Z, Zhao HL. Percutaneous lumbar foraminoplasty and percutaneous endoscopic lumbar decompression for lateral recess stenosis through transforaminal approach: Technique notes and 2 years follow-up. *Clin Neurol Neurosurg* 2016; 143:90-94.
11. Choi G, Modi HN, Prada N, Ahn TJ, Myung SH, Gang MS, Lee SH. Clinical results of XMR-assisted percutaneous transforaminal endoscopic lumbar discectomy. *J Orthop Surg Res* 2013; 8:14.
12. Morgenstern R, Morgenstern C, Yeung AT. The learning curve in foraminal endoscopic discectomy: Experience needed to achieve a 90% success rate. *SAS J* 2007; 1:100-107.
13. Wu XB, Fan GX, Gu X, Shen TG, Guan XF, Hu AN, Zhang HL, He SS. Learning curves of percutaneous endoscopic lumbar discectomy in transforaminal approach at the L4/5 and L5/S1 levels: A comparative study. *J Zhejiang Univ Sci B* 2016; 17:553-560.
14. Hurday Y, Xu B, Guo L, Cao Y, Wan Y, Jiang H, Liu Y, Yang Q, Ma X. Radiographic measurement for transforaminal percutaneous endoscopic approach (PELD). *Eur Spine J* 2017; 26:635-645.
15. Chen X, Cheng J, Gu X, Sun Y, Politis C. Development of preoperative planning software for transforaminal endoscopic surgery and the guidance for clinical applications. *Int J Comput Assist Radiol Surg* 2016; 11:613-620.
16. Choi KC, Kim JS, Ryu KS, Kang BU, Ahn Y, Lee SH. Percutaneous endoscopic lumbar discectomy for L5-S1 disc herniation: transforaminal versus interlaminar approach. *Pain Physician* 2013; 16:547-556.
17. Choi I, Ahn JO, So WS, Lee SJ, Choi IJ, Kim H. Exiting root injury in transforaminal endoscopic discectomy: preoperative image considerations for safety. *Eur Spine J* 2013; 22:2481-2487.
18. Min JH, Kang SH, Lee JB, Cho TH, Suh JK, Rhyu IJ. Morphometric analysis of the working zone for endoscopic lumbar discectomy. *J Spinal Disord Tech* 2005; 18:132-135.